OPEN ACCESS

In situ nanoparticle diagnostics by multi-wavelength Rayleigh-Mie scattering ellipsometry

New Journal of Physics
An Institute of Physics and Deutsche Physikalische Gesellschaft Journal

In situ nanoparticle diagnostics by multi-wavelength Rayleigh–Mie scattering ellipsometry

G Gebauer and J Winter

Institute for Experimental Physics II (Applied Plasma Physics), Ruhr-University Bochum, D-44780 Bochum, Germany
E-mail: GerdGebauer@gmx.de and jw@plas.ep2.ruhr-uni-bochum.de

New Journal of Physics **5** (2003) 38.1–38.17 (http://www.njp.org/)
Received 17 January 2003
Published 28 April 2003

Abstract. We present and discuss the method of multiple-wavelength Rayleigh–Mie scattering ellipsometry for the *in situ* analysis of nanoparticles. It is applied to the problem of nanoparticles suspended in low-pressure plasmas. We discuss experimental results demonstrating that the size distribution and the complex refractive index can be determined with high accuracy and present a study on the *in situ* analysis of etching of melamine–formaldehyde nanoparticles suspended in an oxygen plasma. It is also shown that particles with a shell structure (core plus mantle) can be analysed by Rayleigh–Mie scattering ellipsometry. Rayleigh–Mie scattering ellipsometry is also applicable to *in situ* analysis of nanoparticles under high gas pressures and in liquids.

Contents

1367-2630/03/000038+17$30.00
PII: S1367-2630(03)58495-6

1. Introduction

Nanoparticles are the key to many modern technologies and their applications are rapidly increasing. Examples are pigments in paints and cosmetics, pharmaceuticals, self-cleaning surface coatings, dressed particles in high throughput genomic screening and advanced dispersion materials. There are also processes, however, in which nanoparticle formation has to be avoided. During the fabrication of modern microelectronic devices (chips) as an example, more than 40 consecutive plasma assisted processes of deposition and etching are applied. In plasma processes using reactive gases the formation and growth of nanoparticles may occur. When these particles fall on the wafer, e.g. at the end of one process, they may be easily buried during consecutive steps of deposition and become the reason for a lethal defect in the device. In the jargon of microelectronics they are called 'killer' particles. With the decreasing feature size in microelectronics approaching 10 nm in the near future, very small particles with nanometre size are already becoming critical.

Beyond these applications, nanoparticles play an important role in fundamental research. A new area with a rapidly increasing number of scientific publications are complex plasmas, i.e. plasmas which contain nano- or micrometre sized particles in addition to electrons, ions and neutral atoms or molecules. In plasmas the particles are usually charged and show long-range Coulomb interaction and collective effects leading, for example, to the formation of plasma crystals. Another area is astrophysics, where the identification of dust particles in the interstellar dust clouds often relies on plasma-based simulation experiments with *in situ* particle diagnostics.

For both fundamental and applied problems the availability of a non-invasive *in situ* diagnostic, quantifying size distribution, concentration and material properties of the nanoparticles is of great importance. The diagnostic should cover a size range as large as possible and be sensitive down to a few nanometres. We use the scattering of polarized light from the particles and analysis of the change of polarization. The technique was initially called Mie scattering ellipsometry and combines the features of Mie scattering with that of ellipsometry, a technique often used to characterize the optical properties of thin films. The terminology is not quite appropriate, however. Mie scattering occurs when the wavelength of the light is of the order of the particle size. When visible light is used, the scattering from small particles <100 nm, which is of very high relevance in many processes, is approaching the Rayleigh regime in which the particle is small compared to the wavelength. The method should thus rather be called Rayleigh–Mie scattering ellipsometry.

The first description of a Mie scattering ellipsometric system was given by Hayashi and Tachibana [1]. Later measurements were also reported by Swinkels [2] and Gebauer [3]. As will be evident from the following sections the uniqueness of the data can be very much improved when the experiments are carried out simultaneously at various wavelengths. We thus set up a multi-wavelength system. This allows us also to diagnose in detail complicated particle structures, e.g. layered particles, consisting of a core with a shell of different material, for example.

Although we will discuss in this contribution measurements of particles suspended in a low pressure plasma it should be pointed out that the technique can also be used to diagnose nanoparticles in other media, like air flows at atmospheric pressure or in liquids. In the following we will first describe the model development and the experimental set-up and then discuss results for the example of nanoparticles processed in a low pressure plasma.

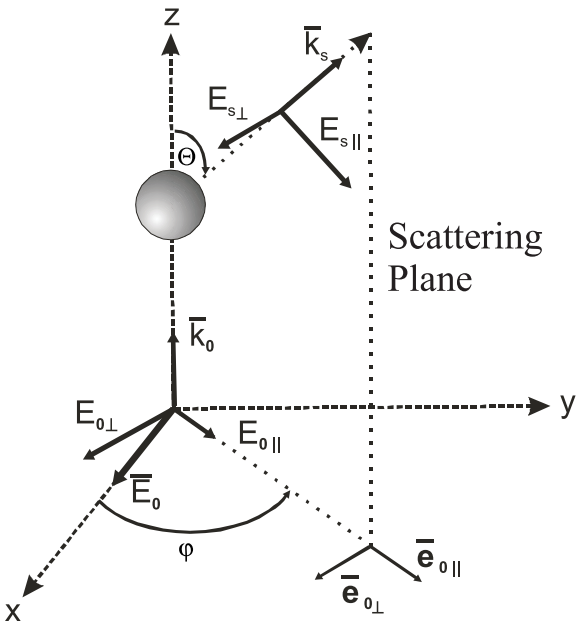

Figure 1. Scattering geometry.

2. Theoretical considerations and models

2.1. Mie ellipsometry of a single particle

Detailed descriptions of Rayleigh and Mie scattering can be found in the papers of Rayleigh [4] and Mie [5] and in the books of Born [6], Kerker [7], van de Hulst [8] and Bohren and Huffmann [9] and will not be repeated here. Following Bohren and Huffmann [9], we assume a scattering geometry as shown in figure 1. A linear polarized electromagnetic wave (polarization along the x axis) is propagating in the z direction and is scattered from a spherical homogeneous particle. The incoming wavevector k_0 and the scattered wavevector k_s define the scattering plane. The scattered electric field vector has components parallel ($E_{||}$) and perpendicular ($E_{\perp}$) to this plane. Θ is the angle between the incoming and the scattered wavevector—the observation is in the direction of k_s. The angle between the scattering plane and the polarization axis x of the incoming wave is defined as φ.

The polarization state of the scattered wave is characterized by the ellipsometric angles Ψ and Δ, which can be measured (see section 2.2). $\tan(\Psi)$ is the ratio between $E_{\parallel}$ and $E_{\perp}$ and Δ is the phase difference between these two components. It can be shown that, under the above assumptions, the following relations hold:

$$\tan(\Psi)\exp(\mathrm{i}\Delta) = \frac{E_{s\parallel}/E_{0\parallel}}{E_{s\perp}/E_{0\perp}} = \frac{S_2}{S_1}. \tag{1}$$

Here $S_1$and S_2 are the elements of a scattering matrix. The functions S_1 and S_2 are described as expansion series of vector harmonic functions. The expansion coefficients depend on the refractive index n of the particle, the refractive index n_0 of the surrounding medium and on the radius r of the particle. Thus r and n may be determined from a measurement of Ψ and Δ. For this purpose we have developed algorithms based on the sketched theoretical background.

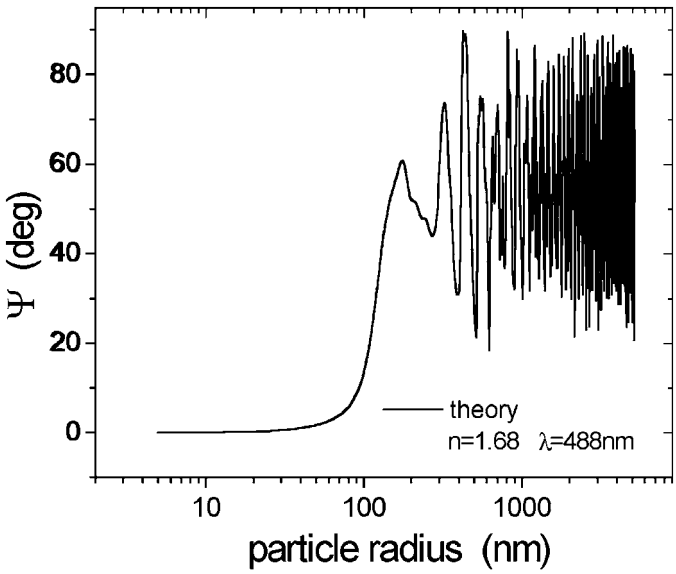

Figure 2. Calculated ellipsometric angle Ψ as a function of the particle radius.

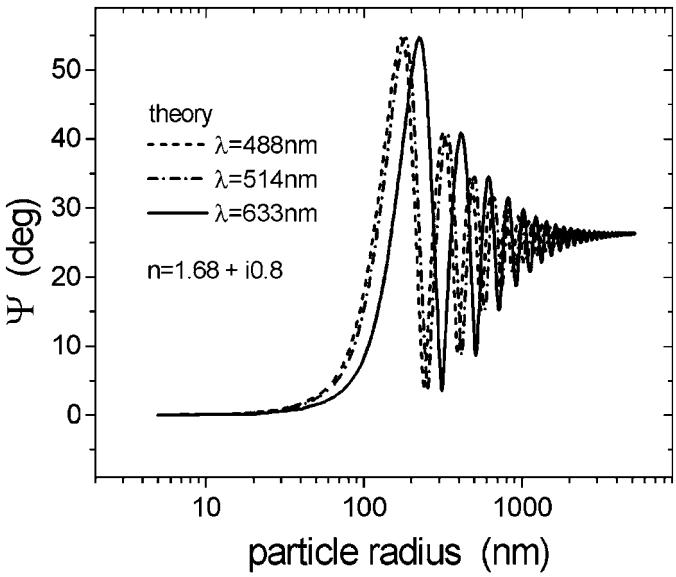

Figure 3. Calculated ellipsometric angle Ψ as a function of the particle radius for different wavelengths.

It should be mentioned here that the scattering properties depend on the shape of the particles. For some more complex shapes of simple geometry (e.g. elongated particles) models are available in the literature. In the following we are considering spherical particles if not otherwise stated. Figure 2 shows a model calculation of the expected variation of Ψ for a dielectric particle as a function of the particle radius.

Above about 300 nm, different radii can be attributed to a measured value of Ψ. The determination is thus not unique. When absorption of light inside the particle occurs, the oscillations are damped, approaching a size-independent value when r exceeds a few

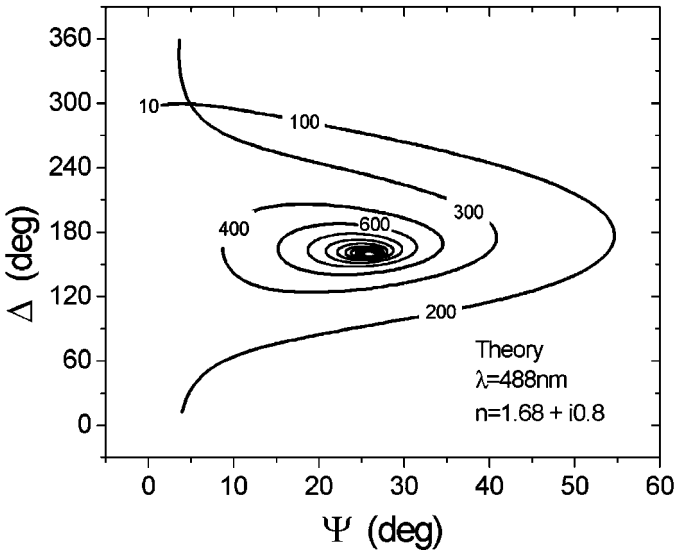

Figure 4. Calculated ellipsometric angle Ψ and Δ as a function of the particle radius. The numerical values on the graph curves show the particle radius in nanometres.

micrometres. A unique range is below about 200 nm, again approaching a size-independent value of Ψ below about 20 nm. An experimental problem for the measurement of small particles arises from the fact, that the scattering cross section decreases rapidly as r^{-6}, reducing the scattered light intensity to extremely small values at small r.

For different wavelengths, the oscillations are shifted with respect to the r axis (see figure 3). Thus an improvement of the uniqueness for the determination of r results from measured Ψ values at different wavelengths. A significant improvement in uniqueness also results from the simultaneous measurement of Ψ and Δ, as shown in figure 4. In the case of the model calculation, uniqueness of the r determination can thus be achieved between about 20 nm and 1 μm.

2.2. Particle size distribution

In many real problems it is rather a distribution of particle sizes than a sharp monodisperse size which has to be analysed. We have added into the algorithm the treatment of a size distribution. Figures 5 and 6 show the computed values of Ψ for different widths of an assumed Gaussian normal distribution of particle radii, and a comparison with the single-particle theory. From figures 5 and 6, it can be recognized that a clear deviation from the single corpuscle theory already occurs at a width of the normal distribution larger than 10 nm. From this fact the conclusion has to be drawn that the size distribution has to be accounted for when interpreting the results. It is also evident from figures 5 and 6 that the ambiguity of a measured Ψ value is further reduced for particle distributions as compared to single particles. The ellipsometric angle Δ is as dependent on the particle size and the size distribution as the ellipsometric angle Ψ. The simultaneous measurement of Ψ and Δ allows the reduction of the ambiguity and is therefore helpful for the determination of the size distribution.

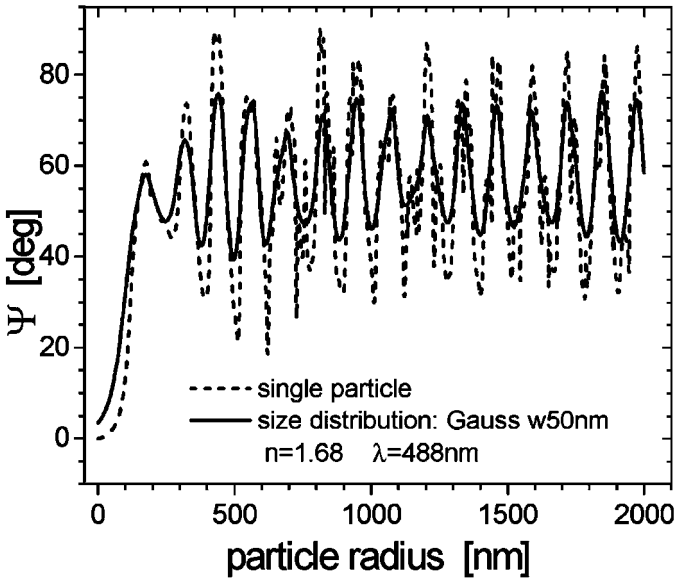

Figure 5. Numerical calculation of Ψ for a single particle and a particle distribution.

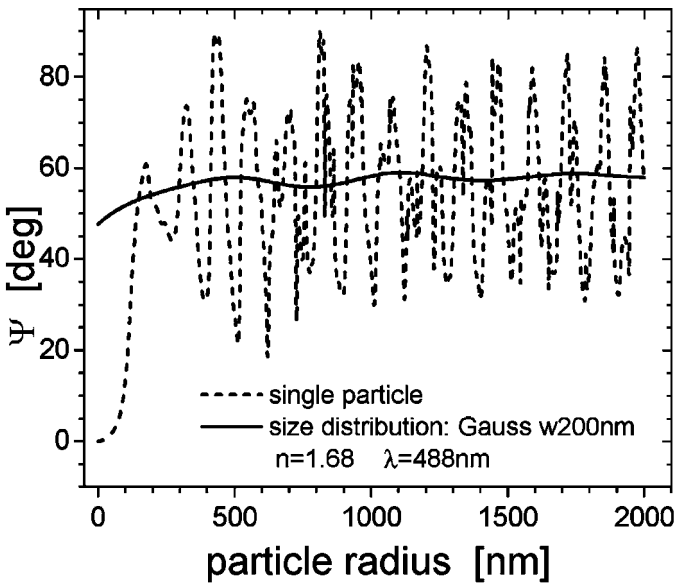

Figure 6. Numerical calculation of Ψ for a single particle and a particle distribution.

2.3. Method for the determination of the size distribution

In the following, we present a method for the determination of particle size distributions that is based on the variation of the polarization of the incoming light. The polarizer through which the laser beam enters into the vessel is turned. This corresponds mathematically to a rotation of the observation position in Mie scattering. The data of Ψ are plotted via the polarizer angle φ. They

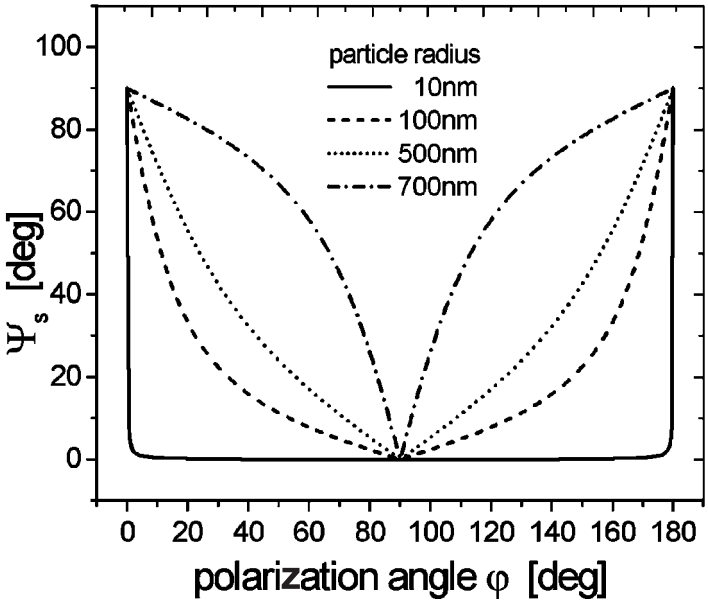

Figure 7. Calculation of Ψ for a single particle.

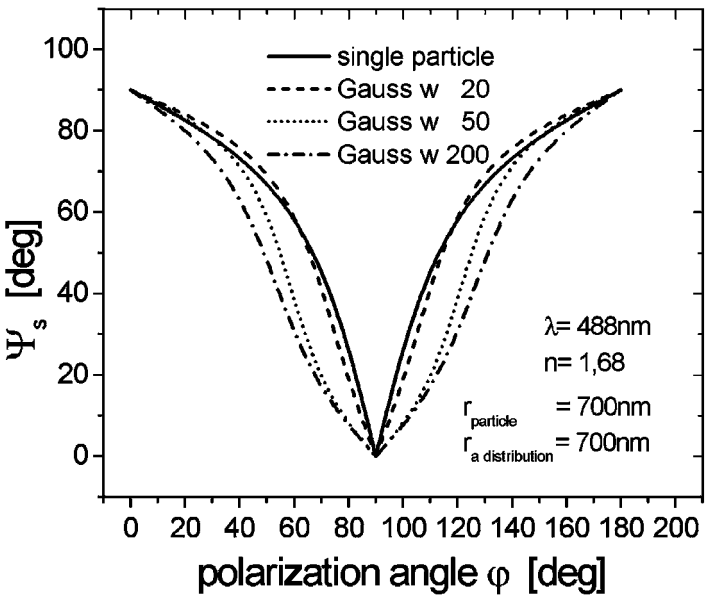

Figure 8. Model calculation of Ψ for a particle distribution.

show a characteristic curve for each particle size distribution. In figure 7 the theoretical curves for single particles with different radii are plotted.

Figure 8 shows the comparison for Gaussian size distributions of varying width and mean radius of 700 nm. The similarity of the curves in figure 8 indicates that a very high measuring accuracy is required for the determination of an unknown size distribution from the measurement.

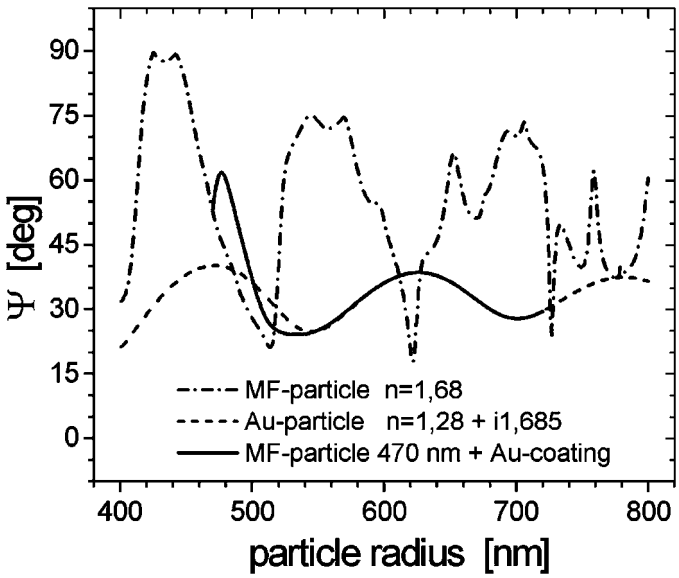

Figure 9. Model calculation of Ψ as a function of the radius for a single pure MF and a single pure Au particle and the variation by a thin gold shell of increasing thickness of MF of 470 nm.

2.4. Multi-layer particles

In basic science, as well as in many applications, the analysis of particles consisting of several layers is of great interest. We assume in the following that the spherical particle has a shell-like structure with a nucleus of radius r_1 and refractive index n_1 covered by a shell of inner radius r_1 and outer radius r_2, refractive index n_2 . The scattering geometry is the same as in figure 1. The scattering process is described by the same formalism as before with the elements of the scattering matrix S_1 and S_2. The expansion coefficients for S_1 and S_2 for this case are given by Bohren and Huffmann [9] and depend on the two radii r_1 and r_2 and on the refractive indices n_1 and n_2. The further steps are as described in section 2.1.

We have calculated the variation of Ψ when a melamine–formaldehyde (MF) particle is coated by a gold layer of increasing thickness. Figure 9 shows the plot of Ψ as a function of radius for a pure MF particle and for a pure gold particle and the variation by the thin gold shell of increasing thickness on MF of 470 nm. The latter curve approaches asymptotically that of pure gold, showing that the MF nucleus is fully shielded after a thickness of 100 nm of gold. The initial variation of Ψ at low gold thicknesses is pronounced and shows that Rayleigh–Mie ellipsometry is a sensitive tool for diagnosing layer thicknesses of a few nanometres.

3. Experimental details

3.1. Experimental set-up

The experimental set-up is shown in figure 10. As discussed in section 2.1, the ambiguity of the results from a Rayleigh–Mie ellipsometric scattering experiment can be reduced by using multiple wavelengths. For this reason we use the three wavelengths 488, 514 and 633 nm from an Ar ion laser and from a He–Ne laser, respectively. They are combined and enter the plasma

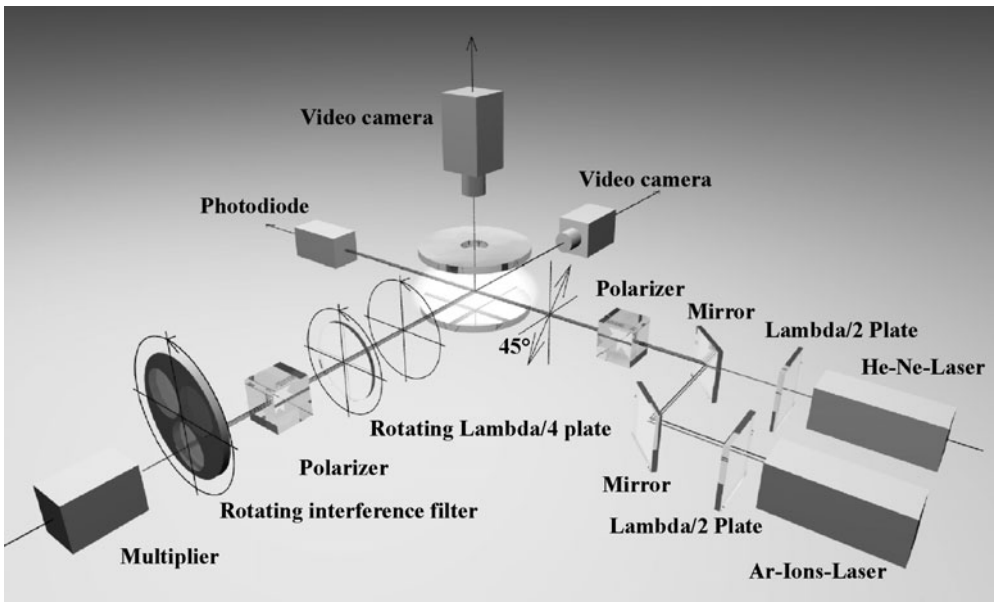

Figure 10. Experimental set-up.

chamber simultaneously with a well-defined polarization state, determined by a polarizer . In order to change the polarization state of the incoming light, this polarizer can be rotated. Two $\lambda/2$ plates right after the lasers allow us to maximize the polarized laser intensity passing through the entrance polarizer. The light scattered from the particles is measured under a well-defined angle, usually under 90° relative to the primary laser beams. The polarization state of the scattered light is defined by its modulation (see [1]–[3]). The modulation of the signal is carried out via the rotation of a $\lambda/4$ plate and via the subsequent filtering of the polarizer signal by continuous rotating interference filters before recording (488, 514 and 633 nm) by a photomultiplier. Using a Fourier analysis the polarization state of the scattered light is determined from the modulated intensity. The rotating $\lambda/4$ plate and filter wheel and the data acquisition are controlled by a computer.

The plasma is established in a capacitively coupled parallel plate reactor with a plate diameter of about 12 cm and a gap width of 5–10 cm. The RF frequency was 13.56 MHz and the power density coupled into the plasma was between 0.025 and 0.5 W cm^{-3}. Particles were introduced into the chamber from the top with a 'salt-shaker'-like dispenser. For the studies described here we used MF and mica particles of a well defined radius, produced by Microparticles GmbH, Berlin. Above a critical size of a few nanometres these particles in a plasma are negatively charged. They are confined in the plasma and repelled from the surface by the sheath potentials. We used a copper ring to establish a radial confining potential component at the lower electrode. Small and light particles accumulate in the bulk plasma where the (positive) plasma potential has a shallow maximum. Heavy particles need larger fields at the sheath edge to be suspended against gravity. We could confine our particles for many hours without any noticeable loss. The optical arrangement was levelled such that the laser beams always interacted with the confined particles. Our monodisperse MF and silicate test particles were usually located in a disc of typically 1.5 cm diameter and 0.5–1.0 mm height at the upper sheath edge of the bottom electrode.

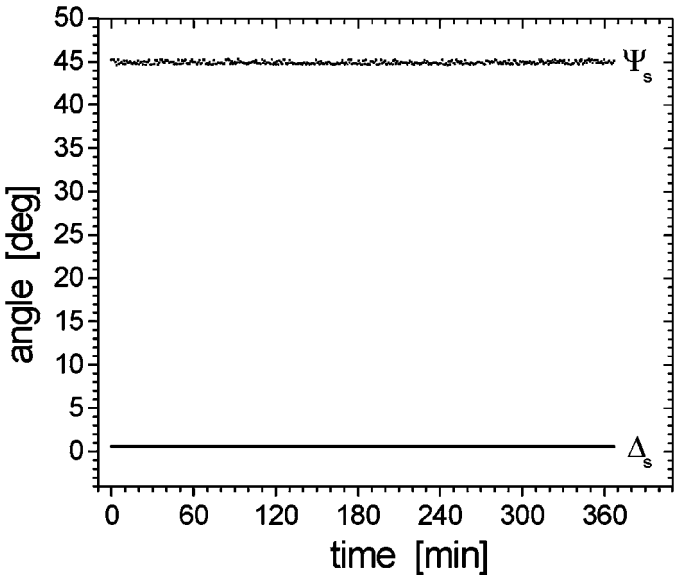

Figure 11. Long-time measurement on mica particles trapped in a plasma.

The signal evaluation requires that the intensity of the signal is stable over the period of signal recording. Intensity fluctuations are caused, e.g., by an irregular particle movement through the measuring volume. Therefore the temporal resolution of the measuring system is an important characteristic for its applicability. The temporal resolution of the system is determined by the rotation frequency of the $\lambda/4$ plate and is 20 ms. For high accuracy of the measurements, averaging is necessary over several single measurements. For quality of the averaging, it is decisive how exactly the individual measurements can be overlaid in a reproducible form without time jitter over the entire measurement period. The long-term stability is characterized by the repeatability of the polarization angles Ψ and Δ. A long-term measurement on mica particles is shown in figure 11. We used mica in this case because, in contrast to MF, the particles there were not affected by plasma–surface interactions over a period of many hours. From this measurement the polarization angles Ψ and Δ of the scattered light can be determined in reproducible form with an accuracy of $\pm 0.5^{\circ}$. From the interpretation of Ψ and Δ it must be considered that the mica particles have the form of plates.

4. Experimental results and discussion

4.1. Particle size distribution and refraction index

The aim of this investigation is the verification of the technique described in section 2.3. We used silica particles (SiO_2) for which the size distribution was specified by the manufacturer, see figure 12. To this size distribution a Gaussian was fitted which is used as a test function for our numerical calculations. The maximum of this Gauss function is at a radius of 1066 nm.

For the numerical determination of the particle size distribution, the maximum of the Gauss function is varied, the known width of the size distribution will be kept constant and the resultant theoretical curves are compared with the experimental data. In figure 13 the relative deviation between the experimental data and the model distribution is plotted for a variation of the value of

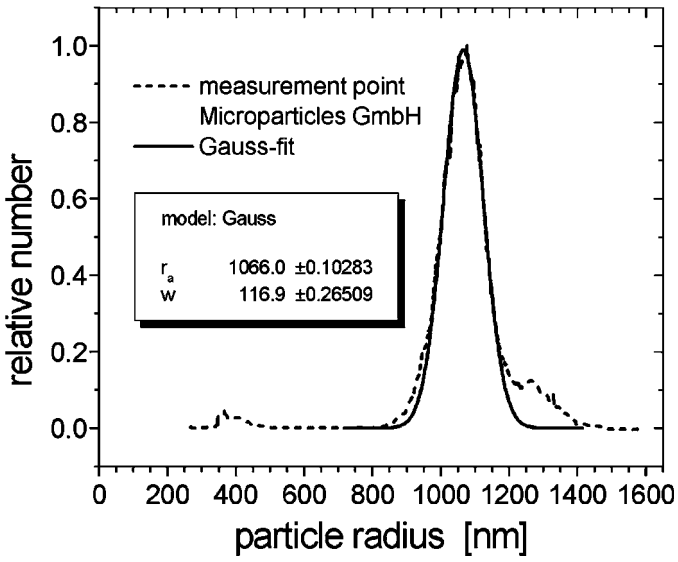

Figure 12. Size distribution measured by the particle manufacture.

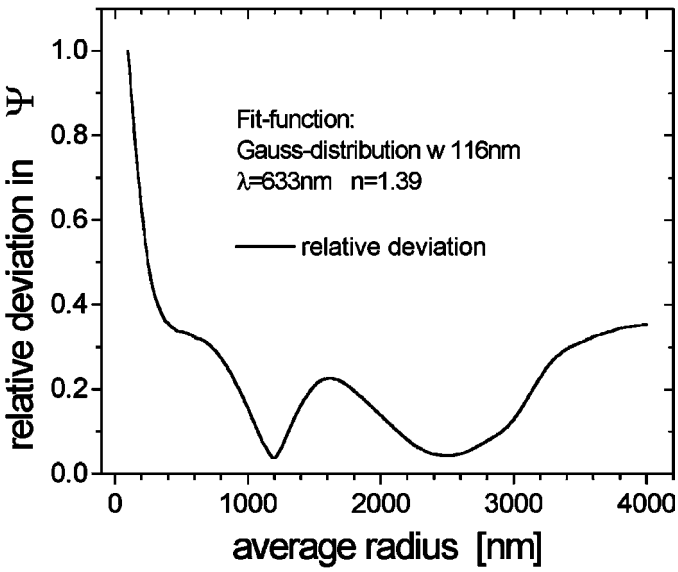

Figure 13. Deviation between measured and modelled size distribution.

the radius at the maximum of the model distribution function. Only two minima appear when the radius is varied up to 4000 nm. They correspond to the position of optimum agreement between measured values and theory. The absolute minimum is at a particle radius of 1195 nm and the second at a radius of 2496 nm. Provided that the input distribution is known within 1000 nm, the first minimum can be clearly assigned to the entry distribution.

The deviation between the manufacturer's specifications and the measured values is due to the assumptions of the Mie algorithm, which presupposes spherical Gauss distributed particles and therefore does not consider the deviations from a normal distribution.

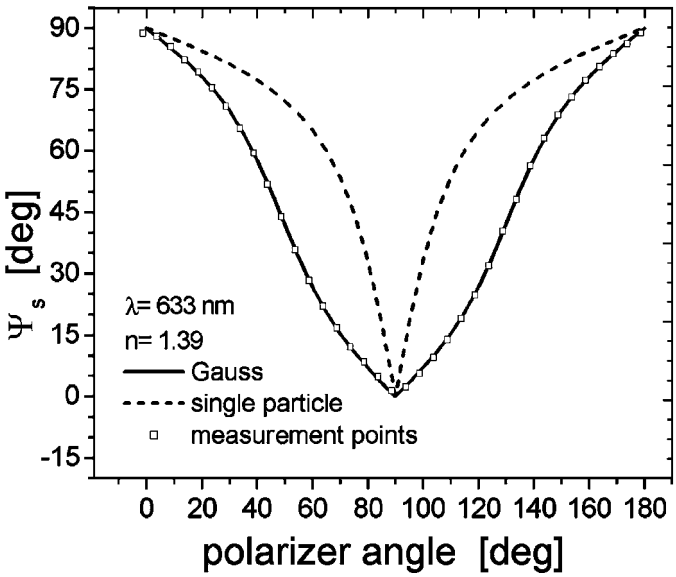

Figure 14. Comparison between measured values and computed size distribution.

In figure 14 the theoretical results of the approximated normal distribution and of one single particle are compared to the measured values in the case of the minimum deviation at 1195 nm. From figure 14 a very good agreement can be seen between the measured values and the theoretical curve using a Gauss distribution with a width of 116 nm. The curve of the monodisperse particles deviates considerably from the measured values. The results of the measurements show that we can determine the size distributions precisely with a deviation of only 10%. Furthermore, we could show that even small distribution widths have to be considered for the interpretation of the results.

The refractive index is determined by a similar numerical procedure as the size distribution. In this case, the refractive index is varied in the code in addition to the other parameters and the known size distribution of the manufacture is used. The manufacturer (Microparticles GmbH, Berlin) indicates an refractive index for silicate particles of 1.37. Different silicate solid states vary between 1.45 and 1.55 [10]. The different values show that the refraction index is different for nanoparticles and solid states.

For a less ambiguous determination of the refractive index, measurements at several wavelengths were carried out. At the wavelengths used, the dispersion of the material is in the range of the measurement error and is thus neglected here. The results are presented in figure 15.

The refractive index is also determined via the minimum deviation between the respective measured values and the theoretical curves. The refractive index for all three wavelengths was determined to be 1.39 ± 0.005.

The results of the measurements show that we can determine the size distributions precisely with a deviation of only 10%. Furthermore, we could show that even small distribution widths have to be considered for the interpretation of the results. Also the refractive index can be determined with very good accuracy.

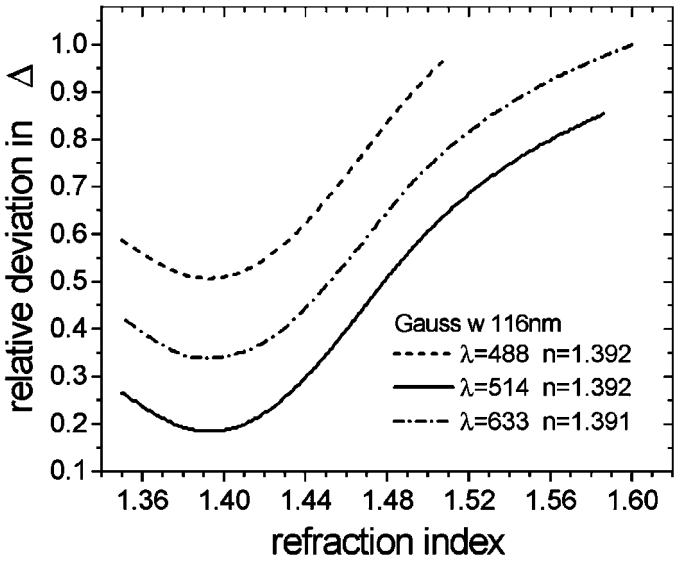

Figure 15. Determination of the refraction index.

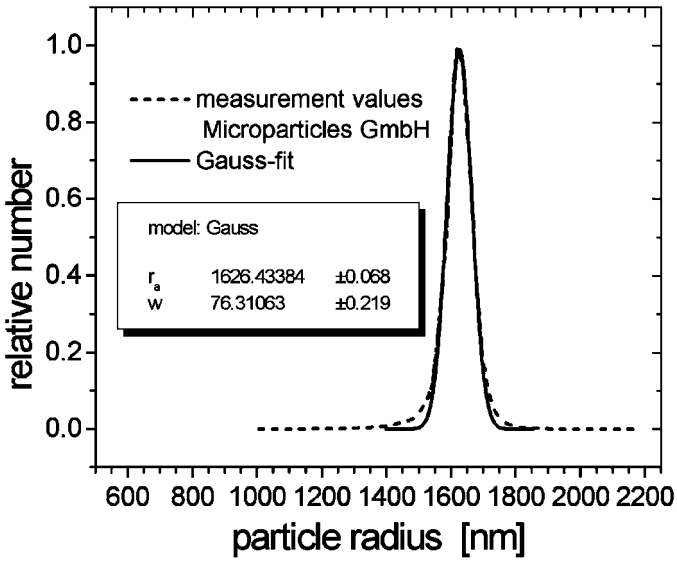

Figure 16. Size distribution measured by the particle manufacturer.

4.2. Etching of MF in an oxygen plasma

We investigated the etching of MF particles suspended in our parallel plate reactor operated in oxygen gas. The plasma was operated at low gas flow rates of a fraction of 1 sccm. In addition to the molecular and atomic oxygen ions a number of chemically active neutral reactive species are formed in such a discharge, in particular O^0 and O_3 . Due to the negative charging of the particles, their surface is exposed to a flux of ionic species, accelerated in the sheath potential around the particles which is of the order of 10 V. The ions and the neutrals mentioned above will react with the MF particles. It is well known that the main reaction product of oxygen plasmas in contact with hydrocarbon based polymers is CO which is volatile and released from the surface.

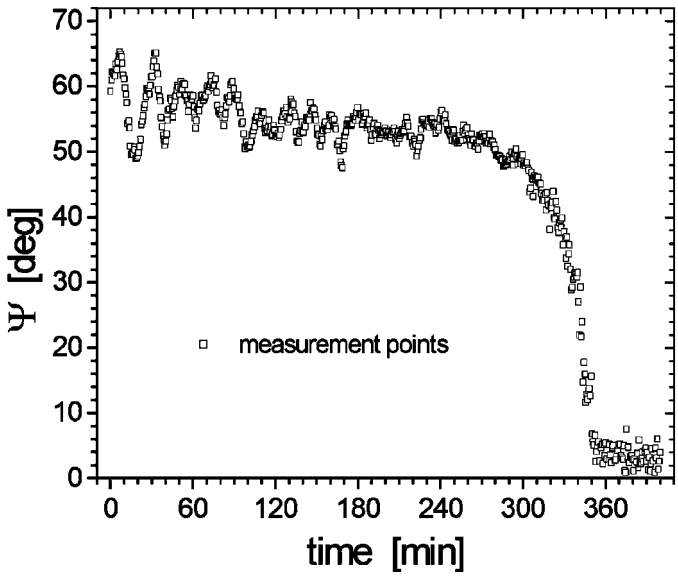

Figure 17. Evolution of the ellipsometric angle Ψ as a function of time during an etching process of MF particles.

We thus expect some physical sputtering and mainly chemical etching, possibly enhanced by the mild ion bombardment of the surface. The size of the particles is expected to decrease as a function of time. It has to be noted that the particles are also exposed to a non-negligible energy flux by the kinetic energy of the impinging ions, the ionization energy liberated and the reaction enthalpy of the chemical processes they may undergo. They may thus have elevated temperatures compared to the neutral gas. Detailed data for the erosion mechanisms of MF are not available to our knowledge.

We used MF particles with a well-defined initial size distribution which can be very well approximated by a Gaussian at $r = 1626$ nm with a width of 76 nm (see figure 16). The measured evolution of the ellipsometric angle Ψ as a function of time is shown in figure 17. During the first 3 h a periodic modulation of the slowly decreasing signal is observed. This may be expected from particles well into the Mie range. The degree of modulation is decreasing as a function of time. The decrease of modulation is a first hint that the distribution width may increase as a function of time (see also figure 5). The modulation becomes less and less significant and after about 5 h a sharp decrease of the measured data is observed.

The sharp decrease occurs when the Rayleigh regime is entered (see, e.g., figure 2). For the evaluation of the data we have assumed that the shape of the particles remains spherical and that the size distribution remains Gaussian, but that the mean size and the full width at half maximum (FWHM) of the distribution function may change. Calculations with a fixed half-width of the size distribution show that a good agreement between calculated and measured data cannot be achieved over the whole range. Much better agreement is achieved when both a decreasing mean size and a continuously increasing width of the distribution are assumed. Figure 18 shows a comparison of measured and calculated data, and figures 19 and 20 show the corresponding variation of r and width, respectively, as a function of the residence time of particles in the oxygen plasma.

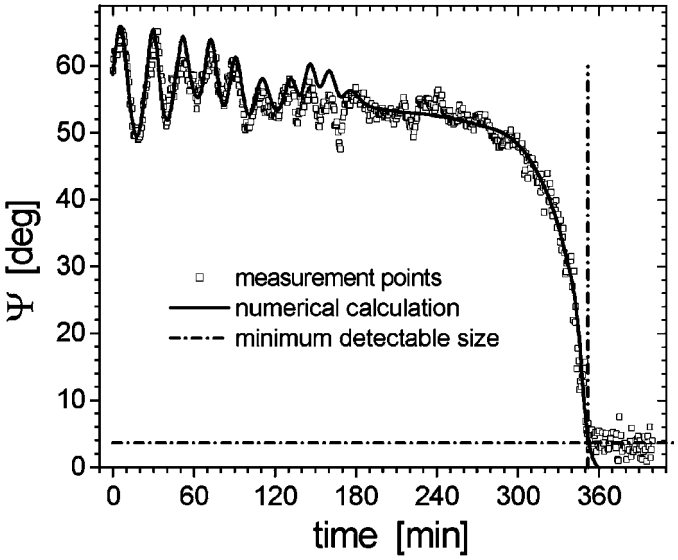

Figure 18. Comparison of measured and calculated data of Ψ as a function of time during the etching process of MF particles.

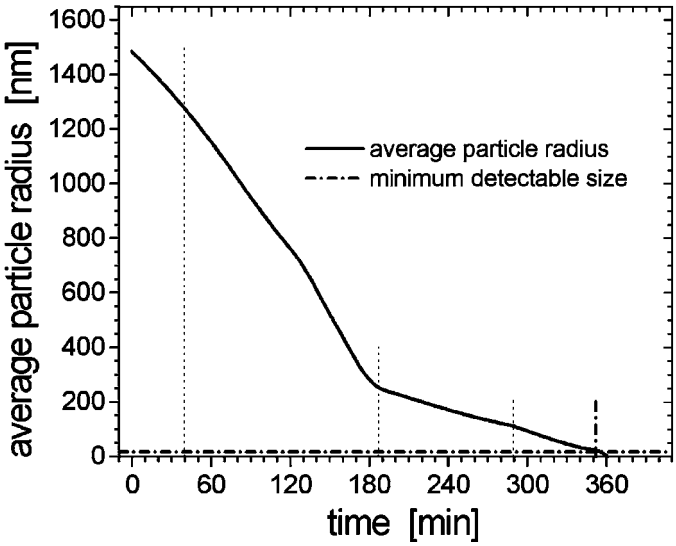

Figure 19. Calculated average particle radius during the etching process.

The initial values of the particle radius and size distribution agree within 10% with those of the known input distribution (figure 16). The minimum detectable size corresponds to about 20 nm. From figure 19 one can see that the particle radius is decreasing more or less linearly at a rate of about 6.8 nm min^{-1} up to 180 min. The etching rate is much slower afterwards (about 1.4 nm min^{-1}). Though the radius changes from the very beginning of the experiment, the width of the distribution changes only slowly initially (first 45 min), indicating essentially a decrease in size of all particles in this phase. Then the width increases at a constant rate of about 0.33 nm min^{-1} up to 180 min.

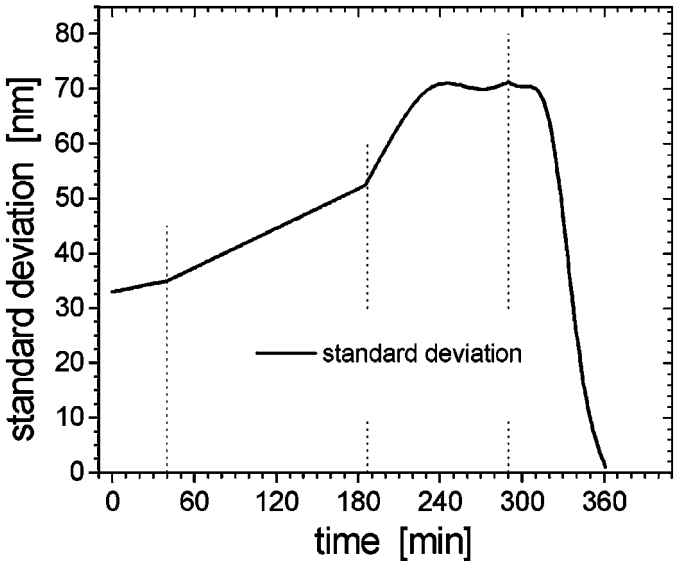

Figure 20. Calculated standard deviation particle of size distribution during the etching process.

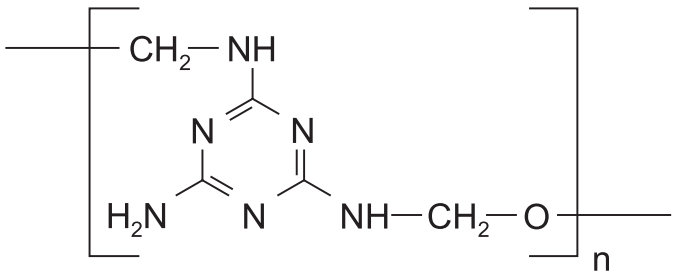

Figure 21. Composite of MF.

Thereafter the rate is increased to about 0.5 nm min^{-1}, reaching a constant value of 158 nm after 290 min. The increasing width indicates non-homogeneous, eventually even size-dependent, etching. This may be due to the quasi-unidirectional ion flow out of the plasma towards the electrode. This introduces a vertical–horizontal asymmetry in the flux impinging on the particles. This would imply a deviation from the spherical shape. Once the particles have become non-spherical an ordering with their elongated axis parallel to the sheath electric field has to be expected.

A progressive change in the chemical composition (see figure 21), a depletion of the methylol and an relative increase in N-rings and azo-groups may very well be responsible for the break in the slope of figure 19 at 180 min. This assumption is supported by the observation of a yellowish–brownish colour change of the discharge close to the particle in the late phase of the experiment (possibly release of NO_x). Due to the very small flow of gas through the reactor a contamination of the discharge gas by the reaction products cannot be excluded. The effects of particle heating have to be considered as well. In order to discuss the measured evolution of radius and distribution more precisely, additional experiments have to be performed.

5. Conclusion

We have realized an experimental set-up of multi-wavelength Rayleigh–Mie scattering ellipsometry. Experimental techniques and algorithms were developed to deduce the size distribution of the particles from the measured ellipsometric angles Ψ and Δ. We have verified the method by comparing the results of a measurement to a known size distribution which was reproduced with very good accuracy. It could be shown that the ellipsometric technique, together with the use of multiple wavelengths and the presence of a size distribution, reduces the ambiguity of classical Mie scattering data significantly. Another quantity which is determined with high accuracy from Rayleigh–Mie scattering ellipsometry is the complex dielectric constant (refractive index and absorption) of nanoparticles. This has been experimentally proven for the example of silicate nanoparticles. We applied Rayleigh–Mie scattering ellipsometry successfully to the *in situ* measurement of the etching of MF nanoparticles in an oxygen plasma. Mean size and particle distribution width change. Such measurements yield information on plasma–surface interactions on a nanoscale. It has been shown that our present set-up is sensitive down to about 10 nm. Methods were developed to analyse particles with a shell structure, i.e. with a core and mantle of materials with different refractive indexes. Measurements are underway. Our present algorithms still assume that the shape of the particles is spherical. Work is underway to generalize the analysis and allow for elongated particles as well.

Although applied for complex plasmas in this study, the technique of Rayleigh–Mie scattering ellipsometry can be used to analyse *in situ* nanoparticle growth, their dielectric properties and size distribution in other environments like atmospheric pressure air jets or liquids.

Acknowledgments

This study was supported by BMBF, MSWF of Nordrhein-Westfalen and SFB 1944.

References

[1] Hayashi Y and Tachibana K 1994 Mie-scattering ellipsometry for analysis of particle behaviors in processing plasmas *Japan. J. Appl. Phys.* **33** L476

[2] Swinkels G 1999 Optical studies of micron-sized particles immersed in a plasma *Proefschrift* Technische Universiteit Eindhoven

[3] Gebauer G 2001 *In situ* nano-partikel diagnostik im plasma durch Mie-ellipsometrie *Dissertation* Ruhr-Universität Bochum

[4] Lord Rayleigh 1964 On the light from the sky, its polarization and colour *Phil. Mag.* **41** 107–20
Lord Rayleigh 1964 *Phil. Mag.* **41** 274–9
Lord Rayleigh 1964 *Phil. Mag.* **41** 1871
(Reprinted in Scientific Papers by Lord Rayleigh, vol I 1869–81 No 8 (New York: Dover))

[5] Mie G 1908 1. Beiträge zur optik trüber Medien speziell kolloidaler Metallösungen *Ann. Phys., Lpz.* **25** 377

[6] Born M 1965 *Optik* (Berlin: Springer)

[7] Kerker M 1969 *The Scattering of Light* (New York: Academic)

[8] van de Hulst H C 1981 *Light Scattering by Small Particles* (New York: Dover)

[9] Bohren C F and Huffmann D R 1983 *Absorption and Scattering of Light by Small Particles* (New York: Wiley)

[10] Landolt–Börnstein Series 1962 *Eigenschaften der Materie in ihren Aggregatzuständen 8. Teil Optische Konstanten* (Berlin: Springer)